HETEROCYCLES, Vol. 106, No. 12, 2023, pp. -. © 2023 The Japan Institute of Heterocyclic Chemistry
Received, 20th October, 2023, Accepted, 13th November, 2023, Published online, 16th November, 2023
DOI: 10.3987/COM-23-14916

SYNTHESIS AND PROPERTIES OF NOVEL THIOPHENE POLYCYCLIC AROMATIC HYDROCARBONS BASED ON PYRENE AND THEIR RADICAL CATIONS

Shunjie Li[a] and Jian Chen[b*]

[a] College of Chemistry and Materials Science, Anhui Normal University, 189 Jiuhuanan Road, Wuhu 241000, China; [b] College of Chemistry and Materials Science, Huaibei Normal University, 100 Dongshan Road, Huaibei 235000, China.

Abstract – Two new thiophene-modified pyrene derivatives, 4,5,9,10-tetra-(2-(5-methyl)thienyl)-2,7-di-*tert*-butylpyrene **(1)** and 4,5,9,10-tetra-(2-(5-methoxy)thienyl)-2,7-di-*tert*-butylpyrene **(2)**, were designed and synthesized via Friedel‑Crafts alkylation and Stille coupling reactions of pyrene. The stable monoradical cations $\mathbf{1}^{\cdot+}$ and $\mathbf{2}^{\cdot+}$ based on the thiophene-modified pyrene derivatives were generated by the one-electron oxidation of the pyrene-based thiophene polycyclic aromatic groups with $Ag[Al(OR_F)_4]$ (OR_F = $OC(CF_3)_3$). Their structures and properties were investigated using ^1H nuclear magnetic resonance spectroscopy, ultraviolet‑visible spectrophotometry, X-ray diffraction, density functional theory calculations, and electron paramagnetic resonance spectroscopy. The electron spin density was mainly concentrated on the pyrene ring, with a minor spillover to the peripheral thienyl moieties. Compound $\mathbf{1}^{\cdot+}$, which is the first reported monoradical cation of thiophene-modified pyrene, is expected to have broad application prospects in the fields of semiconductors and optoelectronic materials.

INTRODUCTION

In the 110 years since Gomberg reported the triphenylmethyl radical,[1] numerous stable radicals have been described.[2] Organic radicals possess open-shell single-electron structures and can easily produce closed-shell compounds with high reactivity through dimerization, hydrogen absorption, disproportionation, and other reactions. Due to their single unpaired electrons, these active substances play important roles in molecular transformation and the preparation of functional materials. Currently,

radical chemistry is closely related to organic chemical reaction mechanisms, as well as the fields of structural chemistry and physics and has been extended to the fields of biomedicine and functional materials.[3] Conjugated aromatic compounds have been widely studied in academic and industrial practice due to their electronic and photoelectric properties. These compounds can be used to prepare organic field effect transistors (OFETs), organic photovoltaic materials, organic light-emitting diodes, and other useful functional materials.[4] Pyrene and its derivatives are well-known polycyclic aromatic hydrocarbons that are mainly used as conductive and photosensitive materials. A nondoped device based on 1,3,5,9-tetra(4-(1,2,2-triphenylvinyl)phenyl)pyrene displayed pure blue emission (λ_{EL}: 468 nm) and a low turn-on voltage (V_{on}: 3.2 V); this excellent performance resulted in a maximum external quantum efficiency of 4.1% and a current efficiency of 7.38 cd/A.[5] Related studies initially focused on thiophene-doped aromatic compounds because the "bridging sulfur" can effectively maximize π-orbital overlap and face-to-face π-π stacking by reducing the degree of freedom of rotation in the molecule. In addition, the thiophene moiety can effectively improve the stability of the compounds.[6]

Many thiophene-modified aromatic compounds, including naphthalene, anthracene, tetrabenzene, and benzothiophene oligomers, have been synthesized and applied in organic semiconductor materials.[7] Thiophene-modified aromatic compounds exhibit relatively large band gaps and low highest occupied molecular orbital (HOMO) energies (E_{HOMO}). These compounds also exhibit abnormally high stability. As electronic materials, these compounds have attracted considerable interest in maximizing π-orbital overlap and improving aromatic stability.

In recent years, the effects of charge on the optical properties and electronic structures of thiophene derivatives have attracted considerable research attention. Thiophene and its derivatives have interesting electrical and optical properties along with excellent environmental stability.[8] When thiophene derivatives are oxidized to the corresponding cations or radical cations, drastic changes in their optical energy levels and transition intensities are observed, although most of these cations are unstable.[9] Compared with neutral molecules, monoradical cations show unique electronic structures along with interesting chemical and magnetism properties.[10] To date, there have been few reports on sulfur-containing aromatic radical cations. The key factor determining the physical and chemical properties of radicals is the electron spin density distribution, which is also an important factor in charge transport in semiconductors. For example, the charge transfer in semiconductor devices is determined by the electron jump process from π-radical ions to adjacent neutral molecules.[11]

Therefore, methods to adjust the electron spin density distribution are important for obtaining useful radical species. Researchers have carried out numerous experiments to control unpaired electrons through various strategies, including the introduction of large steric substituents, extended π-conjugated systems,

and heteroatoms.[12] In this study, we delocalized the single unpaired electron across the entire conjugated system through the introduction of thiophene functional groups. Here, we report the first synthesis and characterization of the novel thiophene-modified pyrene derivative containing 4,5,9,10-tetra(2-(5-methyl)thienyl)-2,7-di-*tert*-butylpyrene **(1)** (Me-TTP) and 4,5,9,10-tetra-(2-(5-methoxy)thienyl)-2,7-di-*tert*-butylpyrene **(2)** (MeO-TTP). We then used $Ag[Al(OR_F)_4]$ (OR_F = $OC(CF_3)_3$) to oxidize **1** and **2** by one-electron to obtain the corresponding monoradical cations and studied their properties. Compared with the neutral precursor molecules, the thiophene-modified pyrene monoradicals showed unique electronic structures and interesting chemical properties. Finally, we discuss the application of the novel compounds **1** and **2** in the fields of semiconductors and optoelectronic materials.

RESULTS AND DISCUSSION

Compared with positions 1, 3, 6, and 8, it is difficult for pyrene to undergo electrophilic substitution reaction at positions 2, 4, 5, 7, 9, and 10; these substitutions must be carried out via indirect electrophilic substitution.[13] First, the Friedel‑Crafts alkylation of pyrene with 2-chloro-2-methylpropane introduced *tert*-butyl moieties at the 2 and 7 positions of pyrene as protecting groups. Next, in carbon tetrachloride solution and the presence of iron powder, 2,7-di-*tert*-butylpyrene was reacted with 6 equivalents of bromine to obtain 4,5,9,10-tetrabromo-2,7-di-*tert*-butylpyrene via bromination.[14] Meanwhile, 2-(tributyltin)-5-methylthiophene was prepared by the lithiation reaction of 2-methylthiophene with *n*-butyllithium and the addition of tributyltin chloride.[15] The key step in the synthesis of 4,5,9,10-tetra(2-(5-methyl)thienyl)-2,7-di-*tert*-butylpyrene **1** was the Stille coupling reaction of 4,5,9,10-tetrabromo-2,7-di-*tert*-butylpyrene and 2-(tributyltin)-5-methylthiophene in the presence of the palladium catalyst tetra(triphenylphosphine)palladium. 4,5,9,10-Tetra(2-(5-methoxy)thienyl)-2,7-di-*tert*-butylpyrene **2** was obtained using a similar method.[16] The synthetic process is shown in Scheme 1.

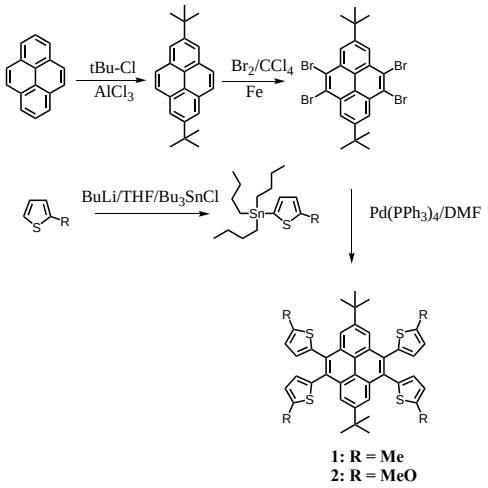

Scheme 1. Synthesis of the neutral compounds Me-TTP (**1**) and MeO-TTP (**2**)

Compounds **1** and **2** were synthesized according to Scheme 1 and characterized by nuclear magnetic resonance (NMR) spectroscopy. In the ^{1}H NMR spectrum, the peaks at δ = 2.37 ppm and δ = 3.83 ppm are the characteristic peaks of methyl and methoxy groups, respectively. Neutral crystals were obtained by solvent evaporation. Under a nitrogen atmosphere, select single crystals with an appropriate size and regular appearance were placed on a glass slide under a N_2 atmosphere for protection, and analyzed by X-ray diffraction using a Bruker D8 Advance X-ray single-crystal diffractometer. The diffraction data were collected with a Mo target at 190 K. The crystal and refinement data of compound **1** are presented in Table 2. We conducted quantitative calculations for neutral crystal **1** to rationalize the structural changes upon one-electron oxidation or reduction. Full geometry optimizations were conducted at the (U)m062x/6-31g(d) level, and the obtained stationary points were verified by frequency calculations. According to previous reports, we found that **1** can hold electrons or lose electrons because of the orbital distribution.[17]

Under the protection of nitrogen, **1** was directly treated with one equivalent of $Ag[Al(OC(CF_3)_3)]_4$ in CH_2Cl_2 as a solvent for two days to obtain a dark green solution. The green filtrate was drained to obtain a dark green powder, which was characterized as monoradical $\mathbf{1}^{\cdot+}[Al(OC(CF_3)_3)_4]^-$. Monoradical $\mathbf{1}^{\cdot+}$, which was obtained in moderate yield, was stable in air at room temperature for more than 10 d. One equivalent of $Ag[Al(OC(CF_3)_3)]_4$ was used to treat **2** in CH_2Cl_2 as a solvent for two days to obtain an inky red solution. The red filtrate was drained to obtain a dark powder, which was characterized as monoradical $\mathbf{2}^{\cdot+}[Al(OC(CF_3)_3)_4]^-$. Monoradical $\mathbf{2}^{\cdot+}$ was stable in air at room temperature for more than 10 d (Scheme 2). The insertion of four methyl and methoxy groups effectively stabilized the free radicals. Notably, as the reaction progressed, the color of **1** gradually darkened, while the color of **2** changed faster, which may be because the methoxy group endowed compound **2** with better solubility. We also compared $AgSbF_6$ with $Ag[Al(OC(CF_3)_3)]_4$ and obtained the same results.

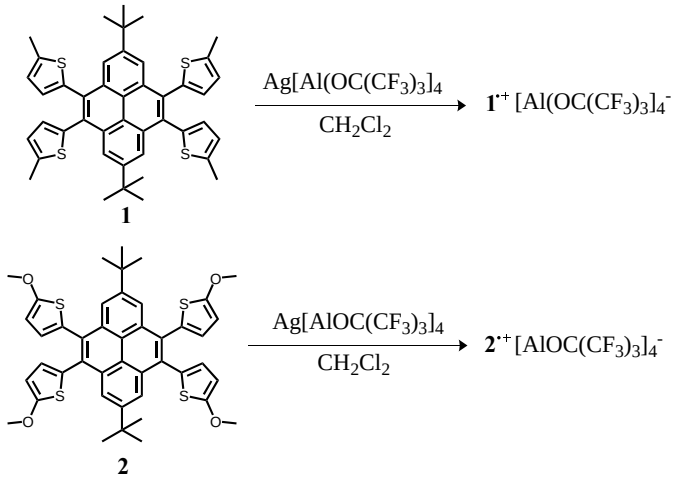

Scheme 2. Synthesis of $\mathbf{1}^{\bullet+}[Al(OC(CF_3)_3)_4]^-$ and $\mathbf{2}^{\bullet+}[Al(OC(CF_3)_3)_4]^-$

Electrochemical Properties

To understand the charge transfer characteristics, ionization potential, and electrochemical stability of the compounds, the redox characteristics of neutral compounds **1** and **2** were studied by cyclic voltammetry. The analytes were dissolved in dichloromethane containing 0.1 M *n*-Bu_4NPF_6 as a supporting electrolyte and analyzed at room temperature at a scanning rate of 100 mV/s. A platinum stick electrode and platinum wire were used as the working electrode and counter electrode, respectively. A Ag/AgCl electrode was used as the reference electrode and was calibrated against ferrocene/ferrocenium (Ag/Ag^+) at the beginning of the experiment. At room temperature, the cyclic voltammogram of **1** showed two quasi-reversible oxidation peaks (**1**, $E_{1/2}^{Ox}$ = 1.10, 1.60 V), indicating that under CV conditions, single cation $\mathbf{1}^{\cdot+}$ and double cation $\mathbf{1}^{2+}$ were stable in solution (Figure 1). Due to the large value of the second oxidation potential of $\mathbf{1}^{\cdot+}$, it was difficult to oxidize this species using conventional oxidants. Therefore, it was difficult to obtain the double cation $\mathbf{1}^{2+}$ through chemical oxidation. According to the CV curve, the onset oxidation potential (E_{Ox}) was 0.29 V (relative to Ag/AgCl). Assuming that the ferrocene/ferrocenium reference energy level is 4.8 eV in a vacuum, the E_{HOMO} value can be estimated from the initial oxidation potential in a cyclic voltammogram.[18] The E_{HOMO} of **1** was calculated to be −5.01 eV using the following equation: $E_{HOMO} = -e(E_{Ox}+4.72)$ (eV). The stability of organic semiconductor materials under oxidation doping is related to their ionization potential (i.e., the E_{HOMO} value in a vacuum). Therefore, the environmental stability can be improved by reducing E_{HOMO} and the p-doping level under an ambient oxygen atmosphere. Compared with those of most current OFET materials,[19] the low E_{HOMO} level of **1** indicated that it has better oxidation stability than traditional p-type semiconductor materials due to the low possibility of oxygen doping.[20]

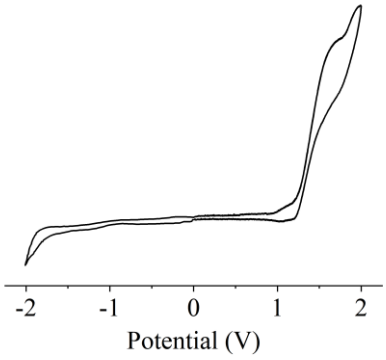

Figure 1. CV curve of neutral compound **1**

Magnetic Properties

We studied the magnetic properties of $\mathbf{1}^{\cdot+}$ using electron paramagnetic resonance (EPR) spectroscopy. First, we diluted a solution of $\mathbf{1}^{\cdot+}[Al(OC(CF_3)_3)_4]^-$ in CH_2Cl_2 to a concentration of 5×10^{-3} mol/l for EPR analysis at room temperature (Figure 2a). The EPR results indicated hyperfine coupling between the single electron of $\mathbf{1}^{\cdot+}$ and the H atom on the pyrene ring. Based on the simulated EPR spectrum, the *g* factor was 2.0033, and the ^1H hyperfine coupling constant was $A(^1H)$ = 2.15 G, 2H. The EPR spectrum of a low-temperature (frozen) solution of $\mathbf{1}^{\cdot+}$ was then measured at 100 K. The spectrum of the one-electron oxidized $\mathbf{1}^{\cdot+}$ showed the characteristics of a diradical (Figure 2b). At the same time, we observed the half-field forbidden transition signal of $\Delta m_s = \pm 2$ at 100 K, and the zero-field splitting value *D* was calculated to be 28.5 G. The EPR spectrum of the solid powder was also measured at 100 K (Figure 2c) and showed both a diradical signal and a half-field signal. Thus, the EPR pattern suggested that the cationic charge was mainly localized on a central pyrene moiety. Not surprisingly, the EPR analysis of $\mathbf{2}^{\cdot+}$ revealed results similar to those of $\mathbf{1}^{\cdot+}$ (Figure 2d). We successfully detected the diradical signal of $\mathbf{2}^{\cdot+}$; at the same time, the low-temperature (frozen) solution EPR spectrum of $\mathbf{2}^{\cdot+}$ also indicated a significant half-field forbidden transition signal with $\Delta m_s = \pm 2$. However, compared to methyl groups, methoxy groups cause splitting at the top of the signal with $\Delta m_s = \pm 1$ in the EPR spectrum to be less pronounced and the line width to increase slightly. The reason for these small differences may be the different electronic effects between methyl and methoxy groups.

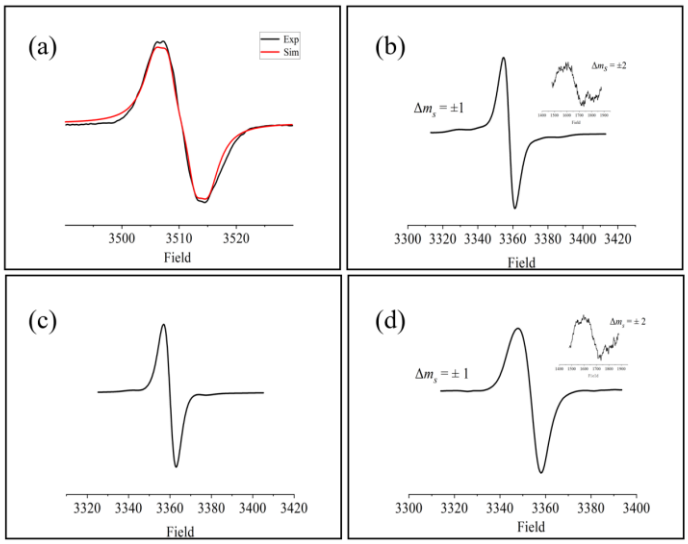

Figure 2. (a) Liquid EPR spectrum of 5×10^{-3} M $\mathbf{1}^{\cdot+}[Al(OC(CF_3)_3)_4]^-$ in CH_2Cl_2 at 298 K; (b) EPR spectrum of 5×10^{-3} M $\mathbf{1}^{\cdot+}[Al(OC(CF_3)_3)_4]^-$ in CH_2Cl_2 at 100 K; (c) Powder EPR spectrum of $\mathbf{1}^{\cdot+}[Al(OC(CF_3)_3)_4]^-$ at 100 K; (d) EPR spectrum of 5×10^{-3} M $\mathbf{2}^{\cdot+}[Al(OC(CF_3)_3)_4]^-$ in CH_2Cl_2 at 100 K

In order to estimate the electronic coupling interaction between the radicals, superconducting quantum interference device (SQUID) measurements of the powder samples of radical cations $\mathbf{1}^{\cdot+}$ and $\mathbf{2}^{\cdot+}$ were carried out (Figure 3). For $\mathbf{1}^{\cdot+}$, the molar paramagnetic susceptibility and temperature, X_mT, was shown to be 0.386 cm^3 K mol^{-1} at room temperature and the maximum value remained at 100 K upon cooling (Figure 3a). It gradually decreases as the temperature is further lowered from 100 K to 2 K (0.04 cm^3 K mol^{-1} at 2 K), indicating an intermolecular interaction. For $\mathbf{2}^{\cdot+}$, X_mT was shown to be 0.375 cm^3 K mol^{-1} from room temperature to 20 K (Figure 3b). It gradually dropped from 20 K to 2 K (0.10 cm^3 K mol^{-1} at 2 K) but faster than $\mathbf{1}^{\cdot+}$, implying a weaker interaction.

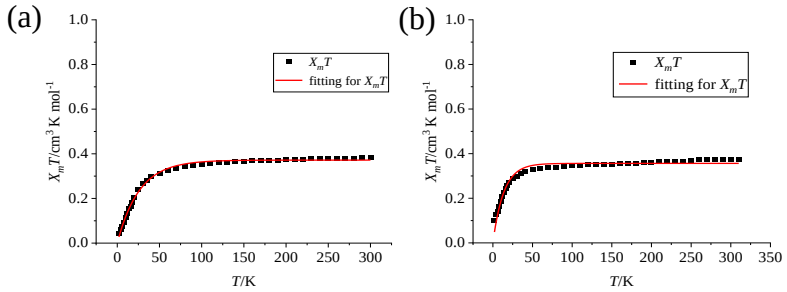

Figure 3. (a) SQUID magnetometry for powder $\mathbf{1}^{\cdot+}[Al(OC(CF_3)_3)_4]^-$ in the warming mode at 1000 Oe; (b) SQUID magnetometry for powder $\mathbf{2}^{\cdot+}[Al(OC(CF_3)_3)_4]^-$ in the warming mode at 1000 Oe

X-Ray Crystallographic Analysis

We collected and analyzed the crystallographic data of compound **1** (Figure 4). Selected bond lengths are shown in Table 1, and the relevant crystal parameters and structural refinement data are provided in Table 2. Due to the addition of the alkyl thiophene group, the central pyrene moiety of the new compound was not completely planar; rather, it was slightly curved. A comparison between the bond length data of **1** and 2,7-di-*tert*-butylpyrene[21] indicated a change in the C–C bond length of the aromatic ring. Upon the addition of thiophene functional groups, the distance between C6–C7 and the two carbon atoms directly connected to the thiophene functional groups increased from 1.348 to 1.353 Å, and the C7–C13 bond length increased from 1.439 to 1.455 Å. Furthermore, the C13–C14 bond length decreased from 1.399 to 1.388 Å, the C22–C23 bond length decreased slightly from 1.422 to 1.415 Å, and the C13–C22 bond length did not change significantly. These changes were conducive to the generation of free radicals and the emergence of double free radical signals. Unfortunately, we did not obtain crystallographic data for free radicals $\mathbf{1}^{\cdot+}$ and $\mathbf{2}^{\cdot+}$, potentially due to the presence of a residue from the tin reagent. Thus, we could not further investigate the effect of electron loss on the structure of the aromatic skeleton.

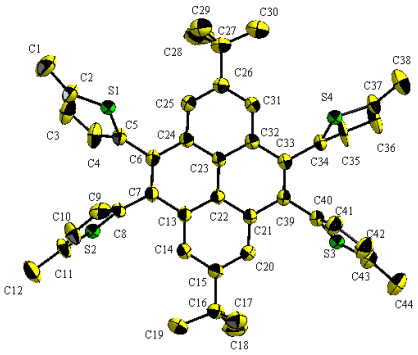

Figure 4. Thermal ellipsoid (50%) drawing of **1**. All hydrogen atoms are not shown for clarity. Selected bond lengths (Å): C13-C14, 1.388(3); C13-C22, 1.415(3); C13-C7, 1.454(3); C32-C31, 1.395(3); C32-C23, 1.417(3); C32-C33, 1.450(3); C14-C15, 1.391(3); C23-C24, 1.414(3); C23-C22, 1.415(3); C21-C20, 1.387(3); C21-C22, 1.422(3); C21-C39, 1.447(3); C20-C15, 1.390(3); C6-C7, 1.353(3); C6-C24, 1.457(3); C25-C24, 1.390(3); C39-C33, 1.357(3); C26-C31, 1.386(3); C26-C25, 1.392(3)

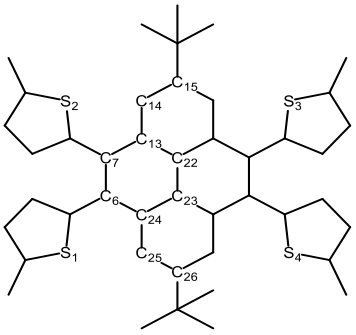

	1	**pyrene**
C13–C14	1.388	1.399
C7–C13	1.455	1.439
C6–C7	1.353	1.348
C13–C22	1.415	1.415
C22–C23	1.415	1.422

Table 1. Selected bond lengths (Å) of compound **1**

Density Functional Theory Calculations

To further explore their electronic properties, we performed quantitative calculations of **1** and $\mathbf{1}^{\cdot+}$ at the (U)m062x/6-31g(d) level. As expected, upon the introduction of 2-methylthiophene functional groups, single unpaired electrons were delocalized across entire conjugated system. Based on the calculation results, we ascribed this delocalization to the change in bond length resulting from the introduction of the electron-rich thiophene group. The highest occupied molecular orbital (HOMO) and lowest unoccupied molecular orbital (LUMO) of compound **1** were completely delocalized throughout the pyrene moiety, indicating that in this unique structure, **1** can simultaneously act as an electron donor and electron acceptor. The spin density distribution of $\mathbf{1}^{\cdot+}$, the singly occupied molecular orbital (SOMO), and the lowest unoccupied molecular orbital (LUMO) were delocalized across the entire molecule; the spin

density on the thiophene ring was partially delocalized, but was relatively large at the pyrene moiety (Figure 5). The monoradical cation $\mathbf{2}^{\cdot+}$ showed similar characteristics.

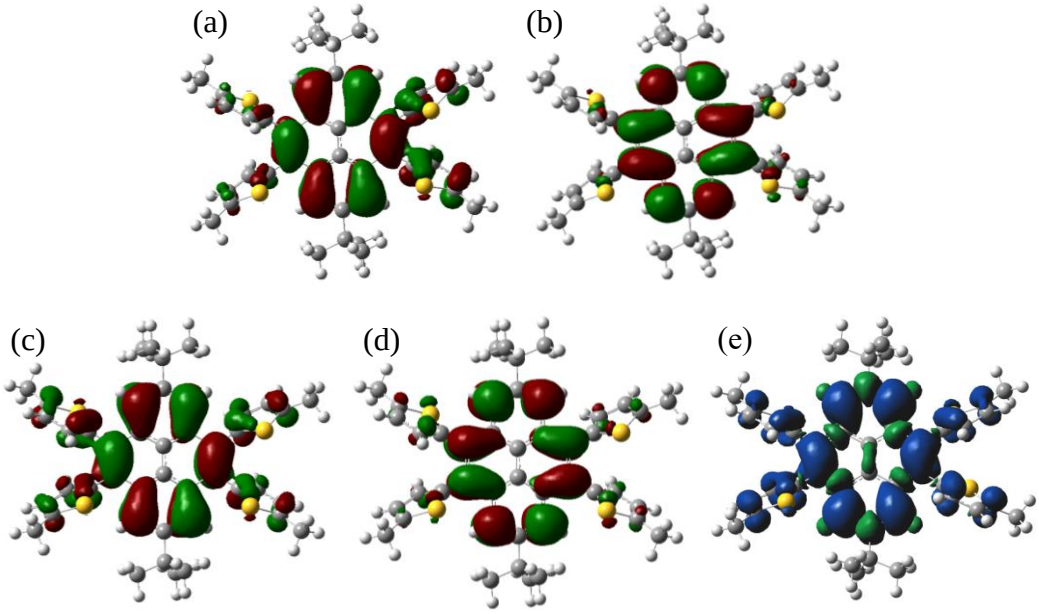

Figure 5. The HOMO of **1** (a) and the LUMO of **1** (b) calculated at the (U)m062x/6-31G(d) level. The SOMO of $\mathbf{1}^{\cdot+}$ (c) and the LUMO of $\mathbf{1}^{\cdot+}$ (d) calculated at the (U)m062x/6-31G(d) level. (e) Spin density map of $\mathbf{1}^{\cdot+}$ calculated at the Um062x/6-31G(d) level

Photophysical Properties

UV–vis spectroscopy is an effective tool for studying the optical properties of radicals.[22] We recorded the UV absorption spectra of compounds **1** and **2** along with their free radical species at room temperature in dilute CH_2Cl_2 (Figure 6). Due to their similar structures, **1** and **2** gave rise to generated similar spectral shapes with nearly the same characteristics (e.g., narrow and strong maximum peaks and fine structures). The conjugated oligomers all showed absorption peaks at high energy (approximately 240 nm) due to thiophene and other aromatic groups.[23] In addition, upon the conversion from **1** to $\mathbf{1}^{\cdot+}$ (and **2** and $\mathbf{2}^{\cdot+}$) the starting point of absorption increased by over 10 nm. A slight redshift in the UV–Vis absorption spectrum is typically observed for free radical compounds compared to the corresponding neutral compounds. In this study, compared with the spectra of neutral substances **1** and **2**, the spectra of $\mathbf{1}^{\cdot+}$ and $\mathbf{2}^{\cdot+}$ exhibited characteristic peaks attributed to radical absorption at 400 nm, further confirming the free radical characteristics of these two compounds. The optical bandgap (ΔE_{opt}) was obtained from the wavelength of absorption onset ($\lambda_{abs\text{-}onset}$) as follows: $\Delta E_{opt} = 1240/\lambda_{abs\text{-}onset}$. Based on the $\lambda_{abs\text{-}onset}$ values of 390 nm for **1** and 420 nm for **2**, the optical bandgaps of **1** and **2** were calculated to be 3.18 and 2.95 eV, respectively. In addition, by comparing **1** and **2**, it was found that the $\lambda_{abs\text{-}onset}$ of **2** with a methoxy substituent was greater

than that of **1** with a methyl substituent, and thus, the optical band gap of **2** was slightly less than that of **1**. In general, a larger bandgap corresponds to higher photodegradation stability.

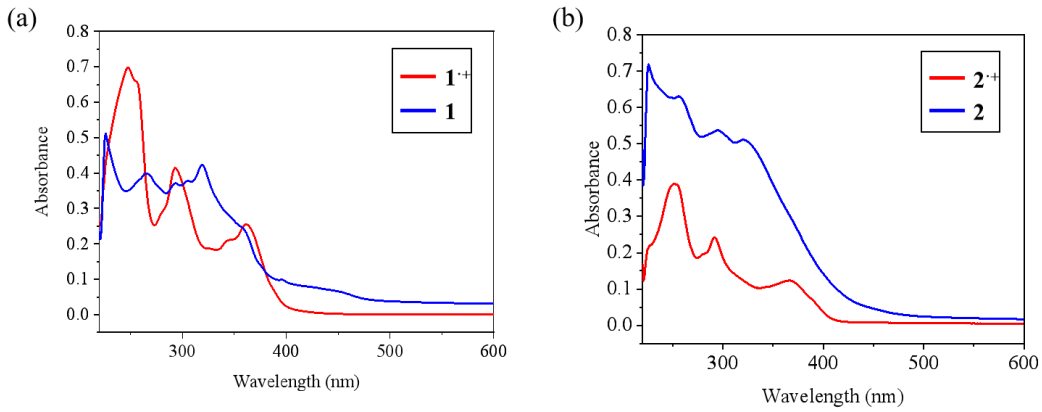

Figure 6. UV–vis absorption spectra of (a) **1** and $\mathbf{1}^{\cdot+}$ in $CHCl_3$ and (b) **2** and $\mathbf{2}^{\cdot+}$ in $CHCl_3$

CONCLUSION

In conclusion, we successfully synthesized the first thiophene-modified pyrene monoradical cations $\mathbf{1}^{\cdot+}$ and $\mathbf{2}^{\cdot+}$ using $Ag[Al(OC(CF_3)_3)_4]$ as the oxidant. EPR spectroscopic analysis and DFT calculations indicated that the cationic free radicals exhibited some unique properties compared with the corresponding neutral thiophene-modified pyrene compounds. Our data revealed that despite the presence of four electron-rich methoxy groups in MeO-TTP the magnetic/optoelectronic properties of these two TTPs were very similar, an unusual finding in comparison with other smaller PAHs. For example, the presence of an electron-rich thiophene group endowed the one-electron oxidized compounds $\mathbf{1}^{\cdot+}$ and $\mathbf{2}^{\cdot+}$ with some diradical properties. In addition, compared to **2**, **1** gave rise to a more pronounced diradical signal at low temperatures, a smaller $\lambda_{abs\text{-}onset}$, and a larger optical bandgap. This work provides a new method for adjusting the electron spin density distribution and physicochemical properties of organic radicals. The photoelectric properties of the monoradical cations also suggest their broad application prospects in the field of photoelectric materials.

EXPERIMENTAL

In this study, the synthesis of air- and water-sensitive compounds was carried out in an inert atmosphere in a glove box using the Schlenk technique. All solvents were treated by drying and degassing before use. Commercially available chemicals were all purchased from Energy Chemical Co., Ltd., while 2-(tributyltin)-5-methylthiophene- and 2-(tributyltin)-5-methoxylthiophene-substituted 2,7-di-*tert*-butyl-

pyrene were synthesized using methods reported in the literature. Melting points were determined on a Büchi B-540/545 hot stage apparatus and were uncorrected. An FA2005 electronic analytical balance was used for weighing compounds. Electron paramagnetic resonance (EPR) spectra were recorded using a Bruker EMX plus-6/1 variable-temperature X-band instrument and simulated using WinEPR Simfonia software. The magnetic property was measured using a MPMS-XL7 SQUID on a sample prepared in a glove box. Ultraviolet‑visible (UV‑Vis) spectra were recorded using a Perkin Elmer Lambda 750 spectrophotometer. Cyclic voltammetry (CV) was carried out in the glove box of a CHI661E chemical workstation. Thin-layer chromatography was performed on silica gel plates (hsgf 255), and the column chromatography products were separated on 300‑400 mesh silica gels. The NMR (400 MHz) spectra were recorded using a Bruker Avance 400 instrument with $CDCl_3$ as the solvent. The ^1H NMR spectral resonance of tetramethylsilane was set as 0.00 ppm, and chemical shifts were expressed in ppm. Crystal structure determination was carried out using a Bruker Smart Apex II CCD X-ray single-crystal diffractometer. The SAINT program was used to integrate the diffraction data and for intensity correction due to the Lorentz and polarization effects. The SADABS program was used for semi-empirical absorption correction. The crystal structure was solved directly, and all non-H atoms were anisotropically refined on *F*2 using the full-matrix least-squares technique in the Shellxl-2014 crystallography software package.[24]

Synthesis of 2-(tributyltin)-5-methylthiophene：

A solution of 5-methylthiophene (5.0 g, 51 mmol) in dry THF was cooled to -78 ℃ under a nitrogen atmosphere, followed by the dropwise addition of *n*-butyllithium (22.44 mL, 2.5 M in hexane) while maintaining a constant temperature. The reaction mixture was stirred for 1 h before the dropwise addition of tributyltin chloride (16.6 g, 51 mmol). After stirring the reaction mixture at -78 ℃ for 1 h, the mixture was warmed to room temperature within 12 h. The reaction was stopped with water (100 mL), and the organic layer was separated. The aqueous layer was extracted with hexane, and the combined organic extracts were dried and concentrated in a vacuum to obtain a yellow oil. The light yellow oil 2-(tributyltin)-5-methylthiophene was obtained as a light yellow oil by distillation. (6.7 g, 54%). ^1H NMR (400 MHz, $CDCl_3$, δ/ppm): δ = 6.97 (d, 1H, *J* = 2.94 Hz), 6.89 (d, 1H, *J* = 2.94 Hz), 2.54 (s, 3H), 1.59-1.52 (m, 6H), 1.38-1.30 (m, 6H), 1.07 (t, 6H, *J* = 8.40 Hz), 0.89 (t, 9H, *J* = 7.29 Hz).

Synthesis of 2-(tributyltin)-5-methoxylthiophene：

2-Methoxythiophene (2.63 g, 23.1 mmol) was placed in dry THF (10 mL) under argon at -78 ℃. A solution of *n*-butyllithium in hexane (2.5 M, 12.4 mL, 31.0 mmol) was then added dropwise. The

suspension was stirred for 80 min until the temperature reached -10 ℃ and then cooled down again to -78 ℃. Tributyltin chloride (7.56 g, 23.2 mmol) was added, and the reaction mixture was allowed to warm up to room temperature within 2 h and then stirred for another 19 h. The mixture was poured into water (30 mL) and extracted with Et_2O (3x15 mL). The organic phase was dried over sodium sulfate. The solvent was removed under reduced pressure affording a brownish oil (7.78 g, 84%). The product was used without further purification in the coupling reaction. ^{1}H NMR (400 MHz, $CDCl_3$, δ/ppm): δ = 6.77 (d, 3*J*(H,H) = 3.5 Hz, 1H), 6.33 (d, 3*J*(H,H) = 3.5 Hz, 1H), 3.89 (s, 3H), 1.66-1.51 (m, 6H), 1.39-1.16 (m, 6H), 1.16-0.96 (m, 6H), 0.94-0.84 (m, 9H).

Synthesis of 1

4,5,9,10-Tetrabromo-2,7-di-*tert*-butylpyrene (0.8 g, 1.27 mmol), 2-(tributyltin)-5-methylthiophene (2.951 g, 7.62 mmol), $Pd(PPh_3)_4$ (176.0 mg, 0.1524 mmol, 2.0 mmol%) and DMF (30 mL) were added to a Schlenk flask. After three freeze-thaw cycles, the mixture was heated to 100 ℃ for 48 h. After cooling to room temperature, the mixture was poured into water and extracted with $CHCl_3$. The solvent was evaporated after drying with magnesium sulfate. Using hexane as the eluent, residue was purified by column chromatography to provide 4,5,9,10-tetra(2-(5-methyl)thienyl)-2,7-di-*tert*-butylpyrene (0.677 g, 83%) in the form of yellow solid. ^{1}H NMR ($CDCl_3$, 400 MHz, δ/ppm): δ = 8.17 (s, 4H), 7.39-7.40 (dd, 4H, *J* = 5.2, 1.4 Hz), 7.05-7.08 (m, 4H), 2.37 (s, 12H), 1.33 (s, 18H). mp > 500 ℃.

Synthesis of 2

4,5,9,10-Tetrabromo-2,7-di-*tert*-butylpyrene (0.8 g, 1.27 mmol), 2-(tributyltin)-5-methoxylthiophene (2.842 g, 7.62 mmol), $Pd(PPh_3)_4$ (176.0 mg, 0.1524 mmol, 2.0 mmol%) and DMF (30 mL) were added to a Schlenk flask. The mixture was heated to 100 ℃ under nitrogen for 48 h. After cooling to room temperature, pour the mixture was poured into water and extracted with CH_2Cl_2. The solvent evaporated after drying with sodium sulfate. Using a mixture of petroleum ether and CH_2Cl_2 as the eluent, the residue was purified by column chromatography to obtain a white solid (0.677 g, 83%). ^{1}H NMR ($CDCl_3$, 400 MHz, δ/ppm): δ = 8.17 (s, 4H), 7.39-7.40 (dd, 4H, *J* = 5.2, 1.4 Hz), 7.05-7.08 (m, 4H), 3.83(s, 12H), 1.33 (s, 18H). mp > 500 ℃.

Synthesis of $1^{\cdot+}$

4,5,9,10-Tetra(2-(5-methyl)thienyl)-2,7-di-*tert*-butylpyrene (0.1 mmol, 0.0700 g), and $AgAl_F$ [Al_F = $Al(OC(CF_3)_3)_4$] (0.1 mmol, 0.1047 g) were placed into a Schlenk flask. Dry CH_2Cl_2 (50 mL) was then

added and reacted overnight. The reaction mixture was filtered, concentrated, and crystallized, giving the desired product. Yield: 0.080 g, 48%.

Synthesis of $2^{\cdot+}$

4,5,9,10-Tetra(2-(5-methoxy)thienyl)-2,7-di-*tert*-butylypyrene (0.1 mmol, 0.0762 g) and $AgAl_F$ (0.1 mmol, 0.1047 g) were added into a Schlenk flask. Dry CH_2Cl_2 (50 mL) was then added and reacted overnight. The reaction mixture was filtered, concentrated, and crystallized, giving the desired product. Yield: 0.089 g, 52%.

Table 2. Crystal Data and Structural Refinement for **1**

	1
formula	$C_{44}H_{42}S_4$
*M*r [g mol^{-1}]	701.07
crystal system	Triclinic
space group	*P1*
Z	2
Temp. (K)	198(2)
a (Å)	10.8608
b (Å)	15.3113
c (Å)	15.4688
α	95.923
β	103.31
γ	108.975
V [Å^3]	2322.50
R^1 (I>2σ(I))	0.0669
wR^2 (all data)	0.2275

$R^1 = \Sigma||F_o| - |F_c||/\Sigma F_o|$, $wR^2 = [\Sigma w(F_o^2 - F_c^2)^2/\Sigma w(F_o^2)^2]^{1/2}$

ACKNOWLEDGEMENTS

The film investigated in this work was fabricated in the Key Laboratory of Functional Molecular Solids Ministry of Education, Anhui Normal University. The authors declare that they have no conflicts of interest.

REFERENCES AND NOTES

1. M. Gomberg, *J. Am. Chem. Soc.*, 1900, **22**, 757.
2. M. Abe, *Chem. Rev.*, 2013, **113**, 7011.
3. H. Guo, Q. Peng, X. Chen, Q. Gu, S. Dong, E. W. Evans, A. J. Gillett, X. Ai, M. Zhang, D. Credgington, V. Coropceanu, R. H. Friend, J. Brédas, and F. Li, *Nat. Mater.*, 2019, **18**, 977.
4. A. R. Murphy and J. M. J. Fréchet, *Chem. Rev.*, 2007, **107**, 1066.
5. F. Xie, H. Ran, X. Duan, R. Han, H. Sun, and J. Hu, *J. Mater. Chem. C*, 2020, **8**, 17450.
6. Y. Didane, G. H. Mehl, A. Kumagai, N. Yoshimoto, C. Videlot-Ackermann, and H. Brisset, *J. Am. Chem. Soc.*, 2008, **130**, 17681.
7. (a) H. S. Kim, Y. H. Kim, T. H. Kim, Y. Y. Nob, S. Pyo, M. H. Yi, D. Y. Kim, and S. K. Kwon, *Chem. Mater.*, 2007, **19**, 4751; (b) H. Meng, F. P. Sun, M. B. Goldfinger, G. D. Jayco, Z. Li, W. J. Marshall, and G. S. Blackman, *J. Am. Chem. Soc.*, 2005, **127**, 2406; (c) J. A. Merlo, C. R. Newman, C. P. Gerlach, T. W. Kelley, D. V. Muyres, S. E. Fritz, M. F. Toney, and C. D. Frisbie, *J. Am. Chem. Soc.*, 2005, **127**, 3997; (d) T. Yamamoto and K. Takimiya, *J. Am. Chem. Soc.*, 2007, **129**, 2224; (e) L. Zöphel, V. Enkelmann, R. Rieger, and K. Müllen, *Org. Lett.*, 2011, **13**, 4506.
8. S. S. Emmi, M. D'Angelantonio, G. Poggi, G. Beggiato, N. Camaioni, A. Geri, A. Martelli, D. Pietropaolo, and G. Zotti, *Res. Chem. Intermed.*, 1998, **24**, 1.
9. P. Bauerle, U. Segelbacher, A. Maier, and M. Mehring, *J. Am. Chem. Soc.*, 1993, **115**, 10217.
10. J. Roncali, P. Leriche, and P. Blanchard, *Adv. Mater.*, 2014, **26**, 3821.
11. L. Ji, M. Haehnel, I. Krummenacher, P. Biegger, F. L. Geyer, O. Tverskoy, M. Schaffroth, J. Han, A. Dreuw, T. B. Marde, and U. H. F. Bunz, *Angew. Chem. Int. Ed.*, 2016, **55**, 10498.
12. Z. Zeng, X. Shi, C. Chi, J. T. López Navarrete, J. Casado, and J. Wu, *Chem. Soc. Rev.*, 2015, **44**, 6578.
13. T. Yamato, A. Miyazawa, and M. Tashiro, *Chem. Ber.*, 1993, **126**, 2505.
14. Y. Miura and E. Yamano, *J. Org. Chem.*, 1995, **60**, 1070.
15. J. T. Pinhey and E. G. Roche, *J. Chem. Soc., Perkin Trans. 1*, 1988, 2415.
16. P. Wilson, D. Lacey, and S. Sharma, *Mol. Cryst. Liq. Cryst.*, 2001, **368**, 279.
17. X. Dong, M. Chen, R. Wang, Q. Ling, Z. Hu, H. Liu, Y. Xin, Y. Yang, J. Wang, and Y. Liu, *Adv. Energy Mater.*, 2023, **13**, 2301006.
18. Q. Sun, H. Wang, C. Yang, and Y. Li, *J. Mater. Chem.*, 2003, **13**, 800.
19. M. L. Tang, A. D. Reichardt, P. Wei, and Z. N. Bao, *J. Am. Chem. Soc.*, 2009, **131**, 5264.
20. W. Porzio, S. Destri, U. Giovanella, M. Pasini, L. Marin, M. D. Iosip, and M. Campione, *Thin Solid Films*, 2007, **515**, 7318.
21. Y. Gong, P. Zhang, Y. Gu, J. Wang, M. Han, C. Chen, X. Zhan, Z. Xie, B. Zou, Q. Peng, Z. Chi, and

Z. Li, *Adv. Opt. Mater.*, 2018, **6**, 1800198.

22. W. Kirmse and J. Kilian, *J. Am. Chem. Soc.*, 1990, **112**, 6400.
23. C. Videlot-Ackermann, J. Ackermann, K. Kawamura, N. Yoshimoto, H. Brisset, P. Raynal, A. E. Kassmi, and F. Fages, *Org. Electron.*, 2006, **7**, 463.
24. Crystallographic data for the structure of **1** have been deposited with the Cambridge Crystallographic Data Center as supplementary publication number CCDC 2302134. These data can be obtained free of charge *via* http://www.ccdc.cam.ac.uk/conts/retrieving.html (or from the CCDC, 12 Union Road, Cambridge CB2 1EZ, UK; fax: +44 1223 336033; e-mail: deposit@ccdc.cam.ac.uk).